The Astrophysical Journal, 868:91 (14pp), 2018 December 1 https://doi.org/10.3847/1538-4357/aae97d

Isothermal Bondi Accretion in Two-component Jaffe Galaxies with a Central Black Hole

Luca Ciotti and Silvia Pellegrini
Department of Physics and Astronomy, University of Bologna, via Piero Gobetti 93/2, I-40129 Bologna, Italy; luca.ciotti@unibo.it
Received 2018 July 27; revised 2018 October 16; accepted 2018 October 16; published 2018 November 27

Abstract

The fully analytical solution for isothermal Bondi accretion onto a black hole (MBH) at the center of two-component Jaffe galaxy models is presented. In a previous work, we provided the analytical expressions for the critical accretion parameter and the radial profile of the Mach number in the case of accretion onto an MBH at the center of a spherically symmetric one-component Jaffe galaxy model. Here we apply this solution to galaxy models where both the stellar and total mass density distributions are described by the Jaffe profile with different scale lengths and masses and to which a central MBH is added. For such galaxy models, all the relevant stellar dynamical properties can also be derived analytically. In these new models, the hydrodynamical and stellar dynamical properties are linked by imposing that the gas temperature is proportional to the virial temperature of the galaxy stellar component. The formulae that are provided allow one to evaluate all flow properties and are then useful for estimates of the scale radius and mass flow rate when modeling accretion onto MBHs at the center of galaxies. As an application, we quantify the departure from the true mass accretion rate of estimates obtained using the gas properties at various distances from the MBH, under the hypothesis of classical Bondi accretion.

Key words: galaxies: elliptical and lenticular, cD – galaxies: ISM – galaxies: nuclei – galaxies: structure – X-rays: galaxies – X-rays: ISM

1. Introduction

Observational and numerical investigations of accretion onto massive black holes (MBHs) at the center of galaxies often lack the resolution to follow gas transport down to the parsec scale. In these cases, the classical Bondi (1952) solution for spherically symmetric, steady accretion of a spatially infinite gas distribution onto a central point mass is commonly adopted; this is the standard reference for estimates of the accretion radius (i.e., the sonic radius) and mass accretion rate (see, e.g., Rafferty et al. 2006; Sijacki et al. 2007; Di Matteo et al. 2008; Gallo et al. 2010; Pellegrini 2010; Barai et al. 2011; Bu et al. 2013; Volonteri et al. 2015; Cao 2016; Choi et al. 2017; Park et al. 2017; Barai & Gouveia Dal Pino 2018; Beckmann et al. 2018; Ramírez-Velasquez et al. 2018). Even though highly idealized, during phases of moderate accretion (in the "maintenance" mode), indeed, the problem can be considered almost steady, and Bondi accretion could provide a reliable approximation of the real situation (e.g., Barai et al. 2012; Ciotti & Ostriker 2012).

However, leaving aside the validity of the fundamental assumptions of spherical symmetry, stationarity, and optical thinness, two major problems affect the direct application of the classical Bondi solution, namely that (1) the boundary values of density and temperature of the accreting gas should be evaluated at infinity; and (2) in a galaxy, the gas experiences the gravitational effects of the galaxy itself (stars plus dark matter) all the way down to the central MBH, and the MBH gravity becomes dominant only in the very central regions, inside the so-called "sphere of influence." The solution commonly adopted in numerical and observational applications to alleviate these problems is to use values of the gas density and temperature "sufficiently near" the MBH, thus assuming that the galaxy effects are negligible. Of course, as the density and temperature of the accreting gas change along the stream lines, the predictions of classical Bondi accretion will also change when based on the density and temperature measured at a finite distance from the MBH. It is therefore of great interest to be able to quantify the systematic effects on the accretion radius and mass accretion rate obtained from the classical Bondi solution, due to measurements taken at a finite distance from the MBH and under the effects of the galaxy potential well.

A first step toward a quantitative analysis of this problem was carried out in Korol et al. (2016, hereafter KCP16), where the Bondi problem was generalized to the case of mass accretion at the center of galaxies, including the effect of electron scattering on the accreting gas. KCP16 then calculated the deviation from the true values of the estimates of the Bondi radius and mass accretion rate, due to adopting as boundary values for the density and temperature those at a finite distance from the MBH and assuming the validity of the classical Bondi accretion solution. In the specific case of Hernquist (1990) galaxies, KCP16 obtained the analytical expression of the critical accretion parameter as a function of the galaxy properties and gas polytropic index γ. However, even for this quite exceptional case, the radial profiles of the hydrodynamical variables remained to be determined numerically. Following KCP16, Ciotti & Pellegrini (2017, hereafter CP17) showed that the whole accretion solution can be given in an analytical way (in terms of the Lambert–Euler W-function) for the isothermal accretion in Jaffe (1983) and Hernquist galaxy models with central MBHs. This meant that for these models, it is not only possible to analytically express the critical accretion parameter, but also the whole radial profile of the Mach number (and then of all the hydrodynamical functions) can be explicitly written. To the best of our knowledge, CP17 provided the first fully analytical solution of the accretion problem onto an MBH at the center of a galaxy.

The galaxy models used in KCP16 and CP17, i.e., the Hernquist and Jaffe models, are not only relevant because it is possible for them to solve the accretion problem but also because of their numerous applications in stellar dynamics. In fact, these models belong to the family of the so-called

Table 1.
Comparison with Earlier Works

	KCP16	CP17	This Paper (CP18)
Galaxy models	Hernquist (1990)	Hernquist (1990), Jaffe (1983)	Two-component JJ (CZ18)
Accretion	Polytropic ($1 \leqslant \gamma \leqslant 5/3$)	Isothermal	Isothermal ($T_\infty = \beta T_V$)
Number of sonic points	One or two	One or two (Hernquist), one (Jaffe)	One
λ_t	Analytic[a]	Analytic	Analytic
Sonic radius	Analytic[a]	Analytic	Analytic
Mach number profile	Numerical	Analytic	Analytic

Note.
[a] The general expression can be found as a function of γ, but only special (asymptotic) cases are given explicitly.

γ-models (Dehnen 1993; Tremaine et al. 1994) and are known to reproduce very well the radial trend of the stellar density distribution of real elliptical galaxies and the bulge component of spiral galaxies; at the same time, their simplicity allows for analytical studies of one- and two-component galaxy models (e.g., Carollo et al. 1995; Ciotti et al. 1996; Ciotti 1999). In particular, Ciotti & Ziaee Lorzad (2018, hereafter CZ18), expanding a previous study by Ciotti et al. (2009), presented spherically symmetric two-component galaxy models (hereafter JJ models), where the stellar and total mass density distributions are both described by the Jaffe profile with different scale lengths and masses, and an MBH is added at the center. The orbital structure of the stellar component is described by the Osipkov–Merritt anisotropy (Merritt 1985). Moreover, the dark matter halo (resulting from the difference between the total and stellar distributions) can reproduce the Navarro et al. (1997, hereafter NFW) profile remarkably well over a very large radial range and down to the center. Among other properties, for the JJ models, the solution of the Jeans equations and the relevant global quantities entering the virial theorem can be expressed analytically. Therefore, the JJ models offer the unique opportunity to have a simple yet realistic family of galaxy models with a central MBH, allowing for both the fully analytical solution of the Bondi (isothermal) accretion problem and the fully analytical solution of the Jeans equations; all this then permits a simple joint study of stellar dynamics and fluid dynamics without resorting to ad hoc numerical codes.

This paper is organized as follows. In Section 2, we recall the main properties of the Jaffe isothermal accretion solution, and in Section 3, we list the main properties of the JJ models. In Section 4, we show how the structural and dynamical properties of the stellar and dark matter components can be linked to the parameters appearing in the accretion solution. In Section 5, we examine the departure of the estimate of the mass accretion rate from the true value when the estimate is obtained using as boundary values for the density and temperature those at points along the solution at a finite distance from the MBH. The main conclusions are summarized in Section 6.

2. Isothermal Bondi Accretion in Jaffe Galaxies with a Central MBH and Electron Scattering

Following KCP16, and in particular the full treatment of the isothermal case in CP17, we shortly recall here the main properties of isothermal Bondi accretion in the potential of a Jaffe galaxy hosting an MBH at its center. Table 1 summarizes the main assumptions and outcomes of KCP16 and CP17 compared to what is done in this work.

2.1. The Classical Bondi Solution

In the classical Bondi problem, the gas is perfect, has a spatially infinite distribution, and is accreting onto an MBH of mass $M_{\rm BH}$. The gas density and pressure are linked by the polytropic relation

$$p = \frac{k_{\rm B}\rho T}{\langle\mu\rangle m_{\rm p}} = p_\infty \tilde{\rho}^\gamma, \quad \tilde{\rho} \equiv \frac{\rho}{\rho_\infty}, \tag{1}$$

where γ is the polytropic index ($\gamma = 1$ in the isothermal case), $m_{\rm p}$ is the proton mass, $\langle\mu\rangle$ is the mean molecular weight, $k_{\rm B}$ is the Boltzmann constant, and p_∞ and ρ_∞ are, respectively, the gas pressure and density at infinity. The sound speed is $c_{\rm s} = \sqrt{\gamma p/\rho}$, and of course, in the isothermal case, it is constant, $c_{\rm s} = c_\infty$, its value at infinity.

The time-independent continuity equation is

$$4\pi r^2 \rho(r) v(r) = \dot{M}_{\rm B}, \tag{2}$$

where $v(r)$ is the modulus of the gas radial velocity, and $\dot{M}_{\rm B}$ is the time-independent accretion rate onto the MBH. An important scale length of the problem, the so-called Bondi radius, is naturally defined as

$$r_{\rm B} \equiv \frac{GM_{\rm BH}}{c_\infty^2}; \tag{3}$$

we stress that the Bondi radius remains defined by the equation above independently of the presence of the galactic potential. After introducing the normalized quantities

$$x \equiv \frac{r}{r_{\rm B}}, \quad \mathcal{M}(r) = \frac{v(r)}{c_{\rm s}(r)}, \tag{4}$$

where $\mathcal{M}$ is the Mach number, Equation (2) determines the accretion rate for the assigned $M_{\rm BH}$ and boundary conditions,

$$x^2 \tilde{\rho}(x) \mathcal{M}(x) = \frac{\dot{M}_{\rm B}}{4\pi r_{\rm B}^2 \rho_\infty c_\infty} \equiv \lambda, \tag{5}$$

where λ is the dimensionless accretion parameter. In the isothermal case, the classical Bondi problem (e.g., KCP16) reduces to the solution of the following system:

$$\begin{cases} g(\mathcal{M}) = f(x) - \Lambda, & \Lambda \equiv \ln\lambda, \\ g(\mathcal{M}) \equiv \frac{\mathcal{M}^2}{2} - \ln\mathcal{M}, \\ f(x) \equiv \frac{1}{x} + 2\ln x. \end{cases} \tag{6}$$

As is well known, Λ cannot be chosen arbitrarily; in fact, both $g(\mathcal{M})$ and $f(x)$ have a minimum, and

$$\begin{cases} g_{\min} = \frac{1}{2}, & \text{for } \mathcal{M}_{\min} = 1, \\ f_{\min} = 2 - 2\ln 2, & \text{for } x_{\min} = \frac{1}{2}. \end{cases} \tag{7}$$

Solutions of Equation (6) exist only for $g_{\min} \leqslant f_{\min} - \Lambda$, i.e., for $\Lambda \leqslant \Lambda_{\rm cr} \equiv f_{\min} - g_{\min}$, which in turn is equivalent to the condition

$$\lambda \leqslant \lambda_{\rm cr} = \frac{e^{3/2}}{4}. \tag{8}$$

Along the critical solutions, i.e., the solutions of Equation (6) for $\lambda = \lambda_{\rm cr}$, $x_{\min}$ marks the position of the sonic point, i.e., $\mathcal{M}(x_{\min}) = 1$. For $\lambda < \lambda_{\rm cr}$ instead, two regular subcritical solutions exist, one everywhere subsonic and one everywhere supersonic, with the respective maximum and minimum value of $\mathcal{M}(x)$ reached at $x_{\min}$.

Summarizing, the solution of the classical Bondi problem requires one to determine $x_{\min}$ and so $\lambda_{\rm cr}$, and possibly to obtain the radial profile $\mathcal{M}(x)$ for a given $\lambda \leqslant \lambda_{\rm cr}$ (see, e.g., Bondi 1952; Frank et al. 1992; KCP16; CP17). Once λ is assigned and $\mathcal{M}(x)$ is known, all functions involved in the accretion problem are known from Equations ((1) and (5)): for example, along the critical solution,

$$\tilde{\rho}(x) = \frac{\lambda_{\rm cr}}{x^2 \mathcal{M}(x)}, \tag{9}$$

while the modulus of the accretion velocity in the isothermal case is $v(r) = c_\infty \mathcal{M}(x)$.

2.2. Isothermal Bondi Accretion (with Electron Scattering) in Jaffe Galaxies

The classical Bondi problem can be generalized by including the effects of radiation pressure due to electron scattering and the additional gravitational field of the host galaxy. In fact, the accretion flow can be affected by the emission of radiation near the MBH that exerts an outward pressure (see, e.g., Mościbrodzka & Proga 2013 for a study of the irradiation effects on the flow). In the optically thin case, the radiation feedback is implemented as a reduction of the gravitational force of the MBH by the factor

$$\chi \equiv 1 - \frac{L}{L_{\rm Edd}}, \tag{10}$$

where L is the accretion luminosity, $L_{\rm Edd} = 4\pi c G M_{\rm BH} m_{\rm p}/\sigma_{\rm T}$ is the Eddington luminosity, and $\sigma_{\rm T} = 6.65 \times 10^{-25}$ cm^2 is the Thomson cross section. Note that the maximum luminosity remains equal to $L_{\rm Edd}$ as defined above, even in presence of the potential of the host galaxy. As shown in KCP16 and CP17 (see also Lusso & Ciotti 2011), for the Bondi problem on an isolated MBH, the critical value $\lambda_{\rm cr}$ and the mass accretion rate modified by electron scattering can be calculated analytically, with the new critical parameter given by $\chi^2 \lambda_{\rm cr}$.

The more general problem of Bondi accretion with electron scattering in the potential of a galaxy hosting a central MBH was addressed in KCP16 and CP17. In particular, it was shown that there is an analytical expression for $x_{\min}$ in the isothermal case in Jaffe galaxies with a central MBH and in the generic polytropic case for Hernquist galaxies with a central MBH; thus, in both cases, it is possible to determine, also in the presence of radiation pressure, the value of the critical accretion parameter (that we now call $\lambda_{\rm t}$). For Hernquist galaxies, the polytropic problem leads to the solution of a cubic equation, producing one or two sonic points (depending on the specific choice of the galactic parameters), while in the isothermal Jaffe case, the relevant equation is quadratic, and only one sonic point exists independently of the galaxy parameters. In addition, CP17 showed that isothermal Bondi accretion cannot be realized in Hernquist galaxies with $M_{\rm BH} = 0$ (or $\chi = 0$), while it is possible in a subset of Jaffe galaxies (provided a simple inequality is satisfied among the galaxy parameters). Summarizing, since $\mathcal{M}$ is also given analytically in the isothermal case, a fully analytical solution exists for isothermal accretion onto MBHs at the center of Hernquist and Jaffe galaxies. However, due to the complications of Bondi accretion in Hernquist galaxies, and given that two-component JJ models with a total Jaffe potential and central MBH have been recently presented (CZ18), in the rest of the paper, we restrict discussion to the case of two-component Jaffe galaxies. Of course, the existence of the analytical accretion solution for the one-component Hernquist model with a central MBH guarantees that a similar analysis could be done for the two-component Hernquist analogs of JJ models.

In the remainder of the section, we recall the main properties of isothermal Bondi accretion in a Jaffe total potential with a central MBH (CP17); in Section 4, these will be used to address the problem of accretion in JJ models. The gravitational potential of a Jaffe density distribution of total mass $M_{\rm g}$ and scale length $r_{\rm g}$ is given by

$$\Phi_{\rm g} = \frac{G M_{\rm g}}{r_{\rm g}} \ln \frac{r}{r + r_{\rm g}}, \tag{11}$$

and, with the introduction of the two parameters,

$$\mathcal{R} \equiv \frac{M_{\rm g}}{M_{\rm BH}}, \quad \xi \equiv \frac{r_{\rm g}}{r_{\rm B}}, \tag{12}$$

the function f in Equation (6) becomes

$$f = \frac{\chi}{x} - \frac{\mathcal{R}}{\xi} \ln \frac{x}{x + \xi} + 2 \ln x, \quad x \equiv \frac{r}{r_{\rm B}}. \tag{13}$$

Note how, for $\mathcal{R} \to 0$ (or $\xi \to \infty$), the galaxy contribution vanishes, and the problem reduces to the classical case. In the limit of $\chi = 0$ ($L = L_{\rm Edd}$),[1] radiation pressure exactly cancels the MBH gravitational field, and the problem describes accretion in the potential of the galaxy only, without electron scattering and an MBH. When $\chi = 1$ ($L = 0$), the radiation pressure has no effect on the accretion flow.

The presence of the galaxy potential and electron scattering changes the accretion rate, which (in the critical case) we now indicate as

$$\dot{M}_{\rm t} = 4\pi r_{\rm B}^2 \lambda_{\rm t} \rho_\infty c_\infty = \frac{\lambda_{\rm t}}{\lambda_{\rm cr}} \dot{M}_{\rm B}, \tag{14}$$

where again $\dot{M}_{\rm B}$ is the classical critical Bondi accretion rate for the same chosen boundary conditions ρ_∞ and c_∞ in Equation (5), and $\lambda_{\rm t}$ is the critical accretion parameter of the

[1] Due to a typo, before their Section 4.1, KCP16 wrote that this case corresponds to $\chi = 1$.

new problem. From the same arguments presented in Section 2.1, λ_t is known once the absolute minimum $f_{\min}(\chi, \mathcal{R}, \xi)$ is known; this, in turn, requires the determination of $x_{\min}(\chi, \mathcal{R}, \xi)$, while the function $g(\mathcal{M})$ is unaffected by the addition of the galaxy potential.

As shown in CP17 for the Jaffe galaxy, the position of the only minimum of f (corresponding to the sonic radius of the critical solution) in Equation (13) is given by

$$x_{\min} \equiv \frac{r_{\min}}{r_B} = \frac{\mathcal{R} + \chi - 2\xi + \sqrt{(\mathcal{R} + \chi - 2\xi)^2 + 8\chi\xi}}{4}, \tag{15}$$

and then one can evaluate $f_{\min} = f(x_{\min})$ and $\ln \lambda_t = f_{\min} - g_{\min}$. In the peculiar case of $\chi = 0$, a solution of the accretion problem is possible only for $\mathcal{R} \geqslant 2\xi$, with

$$x_{\min} = \frac{\mathcal{R} - 2\xi}{2}, \quad \lambda_t = \frac{\mathcal{R}^2}{4\sqrt{e}}\left(1 - \frac{2\xi}{\mathcal{R}}\right)^{2-\mathcal{R}/\xi}. \tag{16}$$

When $\mathcal{R} \to 2\xi$, then $x_{\min} \to 0$ (the sonic point is at the origin), $f_{\min} \to 2\ln\xi$, and, finally, $\lambda_t \to \xi^2/\sqrt{e}$. Note that the $\chi = 0$ case can also be interpreted as the case of a null MBH mass, and the formulae in Equation (16) can be used provided the dependence of $\mathcal{R}$, ξ, and r_B on M_{BH} is factored out and simplified before considering the limit for $M_{BH} \to 0$. Thus, when $M_{BH} = 0$, the condition for the existence of the solution and the position of the sonic radius are

$$\frac{\mathcal{R}}{2\xi} = \frac{GM_g}{2r_g c_\infty^2} \geqslant 1, \quad \frac{r_{\min}}{r_g} = \frac{GM_g}{2c_\infty^2 r_g} - 1. \tag{17}$$

Moreover, even though λ_t in Equation (16) diverges for $M_{BH} \to 0$, the accretion rate given in Equation (14) also remains finite in this case, with a value that can be easily calculated in closed form in terms of the galaxy parameters.

The radial trend of the Mach number for the critical accretion solution of Equation (6) with f in Equation (13) and $\lambda = \lambda_t$ is given by Equation (35) in CP17, that is,

$$\mathcal{M}^2 = -\begin{cases} W(0, -e^{-2f}\lambda_t^2), & x \geqslant x_{\min}, \\ W(-1, -e^{-2f}\lambda_t^2), & 0 < x \leqslant x_{\min}, \end{cases} \tag{18}$$

where W is the Lambert–Euler function, and its relevant properties are given in CP17 (Appendix A; see also Appendix B in CZ18). Note that the subcritical ($\lambda < \lambda_t$) solutions are obtained by using $W(0, z)$ for the subsonic branch and $W(-1, z)$ for the supersonic branch. It is useful to recall that, from the expansion for $x \to 0^+$ of the supersonic branch of $W(-1, z)$ in Equation (18), one has that for $\chi > 0$, $\mathcal{M}(x) \sim \sqrt{2\chi}x^{-1/2}$, while for $\chi = 0$, $\mathcal{M}(x) \sim 2\sqrt{(1 - \mathcal{R}/2\xi)\ln(x/x_{\min})}$ (provided that $\mathcal{R} \geqslant 2\xi$); moreover, the expansion of $\mathcal{M}(x)$ for $x \to \infty$ along the solution with vanishing Mach number at infinity gives $\mathcal{M}(x) \sim \lambda_t e^{-(\chi+\mathcal{R})/x}/x^2$. Once the Mach number radial profile is known, the density profile of the accreting gas is obtained from the analog of Equation (9), with

$$\tilde{\rho}(x) = \frac{\lambda_t}{x^2\mathcal{M}(x)}. \tag{19}$$

3. The Two-component Galaxy Models

We now extend the results in Section 2.1, pertinent to isothermal accretion in the one-component Jaffe model, to the family of two-component JJ models presented in CZ18. These models are characterized by a total density distribution (stars plus dark matter) ρ_g described by a Jaffe profile of total mass M_g and scale length r_g; the stellar density distribution ρ_* is also described by a Jaffe profile of stellar mass M_* and scale radius r_*. The velocity dispersion anisotropy of the stellar component is described by the Osipkov–Merritt formula (Merritt 1985), and an MBH is added at the center of the galaxy. Remarkably, almost all stellar dynamical properties of JJ models with a central MBH can be expressed by analytical functions.

The accretion solution of CP17 for an MBH at the center of a Jaffe potential fully applies to JJ models that are the first family of two-component galaxy models with a central MBH where both the fluidodynamics of accretion and the dynamics of the galaxy can be described in an analytical way. In practice, for isothermal accretion in the JJ models, there is the unique opportunity to easily compare the dynamical properties of the stellar component of the galaxy (velocity dispersion, MBH sphere of influence, etc.) with the accretion flow properties (sonic radius, Bondi radius, critical accretion parameter, Mach number profile, etc.). Here we take an important step further and fix the constant gas temperature T_∞ by using the virial temperature of the stellar component (see Section 3.2 for the full description of the virial temperature and Section 4 for the procedure of linking the gas temperature to the virial temperature). In this way, the JJ models not only provide a more realistic potential well for accretion but also determine the accretion temperature itself, yielding a natural "closure" for the problem and fully constraining the solution. In order to link the properties of the JJ models to the general solution given in CP17, in the following two sections, we introduce the properties of JJ models that are relevant for the present study.

3.1. Structure of the JJ Models

The density distribution of the stellar component of JJ galaxies is

$$\rho_*(r) = \frac{M_* r_*}{4\pi r^2(r_* + r)^2} = \frac{\rho_n}{s^2(1+s)^2}, \quad s \equiv \frac{r}{r_*}, \tag{20}$$

where M_* is the total stellar mass and r_* is the scale length; the effective radius R_e of the stellar profile is $R_e \simeq 0.7447 r_*$. We adopt M_* and r_* as the mass and length scales and define

$$\rho_n \equiv \frac{M_*}{4\pi r_*^3}, \quad \Psi_n \equiv \frac{GM_*}{r_*}, \quad \mu \equiv \frac{M_{BH}}{M_*} \tag{21}$$

as the density and potential scales, and the last parameter measures the MBH-to-galaxy stellar mass ratio. After introducing the structural parameters (cf. Equation (12))

$$\mathcal{R}_g \equiv \frac{M_g}{M_*}, \quad \xi_g \equiv \frac{r_g}{r_*}, \tag{22}$$

we can give the total density distribution (stars plus dark matter) that is also described by a Jaffe profile of scale length r_g and total mass $M_g = M_* + M_{DM}$:

$$\rho_g(r) = \frac{\rho_n \mathcal{R}_g \xi_g}{s^2(\xi_g + s)^2}. \tag{23}$$

Table 2.
List of Defining Parameters for the Galaxy and Accretion Flow

Symbol	Description
Galaxy Structure	
M_g	Total mass
M_*	Stellar mass
M_{BH}	Central MBH mass
r_g	Total density scale length
r_*	Stellar density scale length
σ_V	Stellar virial velocity dispersion
T_V	Stellar virial temperature
μ	M_{BH}/M_*
ξ_g	r_g/r_*
$\mathcal{R}_g$	M_g/M_* $(=\alpha\xi_g, \xi_g \geqslant 1, \alpha \geqslant 1)$
Accretion Flow	
T_∞	Temperature $(=\beta T_V, \beta > 0)$
c_∞	Sound velocity
r_B	Bondi radius
r_{min}	Sonic radius
$\dot{M}_t$	Mass accretion rate
$\mathcal{M}$	Mach number
λ_t	Critical accretion parameter
$\mathcal{R}$	M_g/M_{BH}
ξ	r_g/r_B
x_{min}	r_{min}/r_B
β_c	Critical β $(=3/(2\mathcal{F}_g))$

A summary of the parameters describing the galaxy structure is given in Table 2.

From the request that the dark halo has a nonnegative total mass M_{DM}, it follows that $\mathcal{R}_g \geqslant 1$ (see Equation (22)). The cumulative mass within the sphere of radius r and the associated gravitational potential are given by

$$M_g(r) = \frac{M_*\mathcal{R}_g s}{\xi_g + s}, \quad \Phi_g(r) = \frac{\Psi_n \mathcal{R}_g}{\xi_g} \ln\frac{s}{\xi_g + s}, \tag{24}$$

and the analogous quantities for the stellar component are obtained from Equation (24) for $\mathcal{R}_g = \xi_g = 1$. It also follows that the half-mass (spatial) radius of the total mass profile is r_g, and it is r_* for the stellar mass.

The density distribution ρ_{DM} of the dark halo is given by

$$\rho_{DM}(r) = \frac{\rho_n}{s^2}\left[\frac{\mathcal{R}_g\xi_g}{(\xi_g + s)^2} - \frac{1}{(1+s)^2}\right], \tag{25}$$

so that the ρ_{DM} of the JJ models is not a Jaffe profile, unless the stellar and total length scales are equal ($\xi_g = 1$); the total mass associated with ρ_{DM} is $M_{DM} = M_*(\mathcal{R}_g - 1)$. The request of a nonnegative M_{DM} does not prevent the possibility of an unphysical, locally negative dark matter density for an arbitrary choice of $\mathcal{R}_g$ and ξ_g. In fact, CZ18 showed that the condition to have $\rho_{DM} \geqslant 0$ at all radii is

$$\mathcal{R}_g \geqslant \mathcal{R}_m \equiv \max\left(\frac{1}{\xi_g}, \xi_g\right). \tag{26}$$

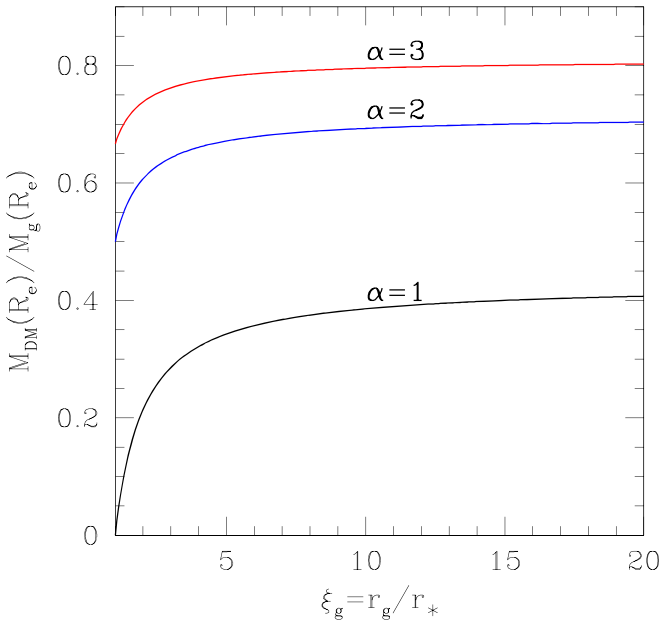

Figure 1. Ratio between the dark mass and the total mass of the JJ models (Equation (28)) within a sphere of radius $r = R_e \simeq 0.75r_*$ as a function of ξ_g for the minimum halo case ($\alpha = 1$, black) and two nonminimum halo cases ($\alpha = 2$, blue; and $\alpha = 3$, red). The dark mass fraction is zero for the one-component (stellar) model, obtained for $\xi_g = 1$ and $\alpha = 1$.

This condition also implies a monotonically decreasing ρ_{DM} with important dynamical consequences. A dark halo of a model with $\mathcal{R}_g = \mathcal{R}_m$ is called a minimum halo model. In the following, we use the parameter α to measure how much $\mathcal{R}_g$ is larger than the minimum halo mass model for assigned ξ_g:

$$\mathcal{R}_g = \alpha\mathcal{R}_m, \quad \alpha \geqslant 1. \tag{27}$$

The special value $\xi_g = 1$ corresponds to the minimum value $\mathcal{R}_m = 1$, i.e., to stellar and total densities that are proportional; in this case, Equation (22) shows that for $\alpha = 1$, there is no dark matter, and one recovers the one-component Jaffe model used in CP17. The properties of the dark halo profile as a function of ξ_g and $\mathcal{R}_g$ are fully discussed in CZ18. We stress that everywhere in this paper, we are restricted to a dark profile more diffuse than the stellar mass, which is obtained for $\xi_g \geqslant 1$; this choice corresponds to the common expectation for real galaxies.[2] From Equations (26) and (27), then, in the following, we always have that $\mathcal{R}_g = \alpha\xi_g$.

It can be of interest for applications to evaluate the dark matter fraction within a sphere of a chosen radius. This amount is easily calculated from Equation (24) as

$$\frac{M_{DM}(r)}{M_g(r)} = 1 - \frac{\xi_g + s}{\alpha\xi_g(1+s)}, \tag{28}$$

where $M_{DM}(r) = M_g(r) - M_*(r)$. Figure 1 shows the ratio between the dark mass and the total mass within a sphere of radius $r = R_e$ as a function of ξ_g for various values of α: the minimum halo case ($\alpha = 1$) and two cases (blue and red curves) with $\mathcal{R}_g > \mathcal{R}_m$. Dark matter fractions below unity are easily obtained, with low fractions (<0.4) for the minimum

[2] The extension of the analysis to the cases $0 \leqslant \xi_g < 1$ would be immediate.

halo case. These low values agree with those required by the modeling of the dynamical properties of nearby early-type galaxies, which indicate that the dark mass within R_e is lower than the stellar mass (e.g., Cappellari et al. 2015).

For what concerns the radial profile of ρ_{DM}, for $r \to \infty$, Equation (25) shows that $\rho_{DM} \sim (\mathcal{R}_g\xi_g - 1)\rho_* \propto r^{-4}$, and so the densities of the dark matter and stars in the outer regions are proportional. For $r \to 0$, in nonminimum halo models, $\rho_{DM} \sim (\mathcal{R}_g/\xi_g - 1)\rho_* \propto r^{-2}$, while in the minimum halo models, $\rho_{DM} \sim 2(1 - 1/\xi_g)s\rho_* \propto r^{-1}$, so that these latter models are centrally baryon-dominated, being $\rho_* \propto r^{-2}$. It is interesting to compare the dark halo profile of JJ models with the NFW profile of total mass M_{DM} that we rewrite for $r < r_t$ (the so-called truncation radius) as

$$\rho_{NFW}(r) = \frac{\rho_n(\mathcal{R}_g - 1)}{f(c)s(\xi_{NFW} + s)^2},$$
$$f(c) = \ln(1 + c) - \frac{c}{1 + c}, \tag{29}$$

where $\xi_{NFW} \equiv r_{NFW}/r_*$ is the NFW scale length r_{NFW} in units of r_*, and $c \equiv r_t/r_{NFW}$. From the considerations above about the behavior of $\rho_{DM}(r)$ at small and large radii, it follows that ρ_{DM} and ρ_{NFW} at small and large radii cannot, in general, be similar. However, in the case of the minimum halo, near the center, $\rho_{DM} \propto r^{-1}$, and it can be proven that ρ_{DM} and ρ_{NFW} can be made identical for $r \to 0$ by fixing

$$\xi_{NFW} = \sqrt{\frac{\xi_g}{2f(c)}} \tag{30}$$

in Equation (29). Therefore, once a specific JJ minimum halo model is considered, Equations (29) and (30) allow one to determine the NFW profile that has the same total mass and central density profile as ρ_{DM}. It turns out that the dark halo profiles of JJ minimum halo models are surprisingly well approximated by the NFW profile over a very large radial range for realistic values of ξ_{NFW} and c (CZ18).

3.2. Dynamics of the JJ Models

CZ18 presented and discussed the analytical solutions of the Jeans equations and all the dynamical properties of Osipkov–Merritt anisotropic JJ models with a central MBH of mass M_{BH}, where the total gravitational potential is

$$\Phi_T(r) = \Phi_g(r) - \frac{\Psi_n\mu}{s}. \tag{31}$$

The radial component of the stellar velocity dispersion tensor is given by $\sigma_r^2(r) = \sigma_g^2(r) + \sigma_{BH}^2(r)$, where σ_g indicates the contribution due to $\Phi_g(r)$, and σ_{BH} is the contribution due to the MBH. Under the assumption of Osipkov–Merritt anisotropy, $\sigma_g(0)$ is coincident with the isotropic case (except for purely radial orbits), independently of the anisotropy radius $r_a > 0$, and is given by

$$\sigma_g^2(0) = \frac{\Psi_n\mathcal{R}_g}{2\xi_g} = \frac{\Psi_n\alpha}{2}, \tag{32}$$

where in the last identity, we use Equation (27) and restrict to $\xi_g \geqslant 1$. Note that the value of $\sigma_g(0)$ is therefore independent of ξ_g for $\xi_g \geqslant 1$, and, in the minimum halo model, it is coincident with that of the one-component (purely stellar) Jaffe model. The leading term of the MBH contribution to σ_r near the center (except for the case of purely radial orbits, $r_a = 0$) coincides with the isotropic case independently of the Osipkov–Merritt anisotropy radius, with

$$\sigma_{BH}^2(r) \sim \frac{\Psi_n\mu}{3s}; \tag{33}$$

at variance with $\sigma_g(r)$, it diverges as μ/r for $r \to 0$. Therefore, in the presence of the central MBH, σ_r is dominated by its contribution, similarly to the projected velocity dispersion (σ_{gp}).

In order to relate the models with observed quantities, it is helpful to consider the projected velocity dispersion in the central regions. CZ18 shows that for $r_a > 0$,

$$\sigma_{gp}(0) = \sigma_g(0), \tag{34}$$

while, independently of the value of $r_a \geqslant 0$,

$$\sigma_{BHp}^2(R) \sim \frac{2\Psi_n\mu}{3\pi}\frac{r_*}{R}, \tag{35}$$

where R is the radius in the projection plane. The two equations above determine a fiducial value for the radius (R_{inf}) of the so-called sphere of influence. We define R_{inf} operationally as the distance from the center in the projection plane where the (galaxy-plus-MBH) projected velocity dispersion $\sigma_p(R)$ equals a chosen fraction ϵ of the projected velocity dispersion of the galaxy in the absence of the MBH. In practice, as $R_{inf} \ll r_*$, and in JJ models without an MBH, the velocity dispersion profile flattens to a constant value, which we define as

$$\sigma_p(R) \simeq \sqrt{\sigma_{BHp}^2(R_{inf}) + \sigma_{gp}^2(0)} = (1 + \epsilon)\sigma_{gp}(0), \tag{36}$$

and from Equations (34) and (35), one has

$$\frac{R_{inf}}{r_*} = \frac{4\xi_g\mu}{3\pi\mathcal{R}_g\epsilon(2 + \epsilon)} = \frac{4\mu}{3\pi\alpha\epsilon(2 + \epsilon)}, \tag{37}$$

where the last identity holds for $\xi_g \geqslant 1$. For realistic values of the parameters, R_{inf} is of the order of a few pc (see Section 5.1 for a more quantitative discussion).

As anticipated in the Introduction, a reasonable estimate of the gas temperature, supported by observations (e.g., Pellegrini 2011), is given by the stellar virial temperature $T_V = \langle\mu\rangle m_p\sigma_V^2/3$ (see Section 4 for a detailed presentation of the link between the gas temperature and T_V). The definition of σ_V comes from the virial theorem that, for the stellar component, reads

$$2K_* = -W_{*g} - W_{*BH}, \tag{38}$$

where $K_* \equiv M_*\sigma_V^2/2$ is the total kinetic energy of the stars, and

$$W_{*g} = -4\pi G\int_0^\infty r\rho_*(r)M_g(r)dr \tag{39}$$

is the interaction energy of the stars with the total gravitational field of the galaxy (stars plus dark matter), and, finally,

$$W_{*BH} = -4\pi GM_{BH}\int_0^\infty r\rho_*(r)dr \tag{40}$$

is the interaction energy of the stars with the central MBH. Note that $W_{*\rm BH}$ diverges because the stellar density profile diverges near the origin as r^{-2}; instead, $W_{*\rm BH}$ converges for γ models with $0 \leqslant \gamma < 2$. Since we will use K_* to evaluate the gas temperature over the whole body of the galaxy (where the MBH effect is negligible), we only consider $W_{*\rm g}$ in the determination of $\sigma_{\rm V}$. Therefore, $\sigma_{\rm V}^2 \equiv -W_{*\rm g}/M_*$, where, from CZ18,

$$W_{*\rm g} = -\Psi_{\rm n} M_* \mathcal{R}_{\rm g} \widetilde{W}_{\rm g}, \quad \widetilde{W}_{\rm g} = \frac{\xi_{\rm g} - 1 - \ln \xi_{\rm g}}{(\xi_{\rm g} - 1)^2}, \tag{41}$$

and $\widetilde{W}_{\rm g}(1) = 1/2$. It follows that $\sigma_{\rm V}^2 = \Psi_{\rm n} \mathcal{R}_{\rm g} \widetilde{W}_{\rm g} = \Psi_{\rm n} \alpha \mathcal{F}_{\rm g}(\xi_{\rm g})$, where we introduced the function $\mathcal{F}_{\rm g}(\xi_{\rm g}) \equiv \xi_{\rm g} \widetilde{W}_{\rm g}$. Note that $\mathcal{F}_{\rm g}(\xi_{\rm g})$ increases from $\mathcal{F}_{\rm g}(1) = 1/2$ to $\mathcal{F}_{\rm g}(\infty) = 1$. In practice, at fixed α and increasing $\xi_{\rm g}$, Equation (27) dictates that $\mathcal{R}_{\rm g}$ increases to arbitrarily large values, but since $\mathcal{F}_{\rm g} \to 1$, $W_{*\rm g}$ and $\sigma_{\rm V}$ (and so the mass-weighted squared escape velocity) remain limited. Physically, this is due to the fact that more massive halos are necessarily more and more extended because of the request for positivity in Equation (26), with a compensating effect on the depth of the total potential. Moreover, from Equations (32) and (34), it follows that $\sigma_{\rm V}^2 = 2\mathcal{F}_{\rm g}(\xi_{\rm g})\sigma_{\rm gp}^2(0)$, so that in JJ models without an MBH, $\sigma_{\rm V}$ is just proportional to the stellar central projected velocity dispersion, and the proportionality constant is a function of $\xi_{\rm g}$ only, with $\sigma_{\rm V} = \sigma_{\rm gp}(0)$ for $\xi_{\rm g} = 1$.

4. Linking Stellar Dynamics to Fluidodynamics

In the general solution of CP17, once the parameters $\mathcal{R}$ and ξ in Equation (12) are assigned and the Jaffe structural scales $M_{\rm g}$ and $r_{\rm g}$ characterizing the total galactic potential are chosen, the gas temperature T_∞ remains fixed, because $\xi = r_{\rm g}/r_{\rm B}$. Therefore, generic values of ξ can easily correspond to unrealistic values of the gas temperature. Clearly, JJ models offer an interesting possibility: as the dynamical properties of the stellar component of the galaxy can be analytically calculated once the total potential (due to stars, dark matter, and a central MBH) is assigned, the virial theorem for the stellar component can be used to compute the virial "temperature" $T_{\rm V}$ of the stars, a realistic proxy for the gas temperature T_∞; then, the CP17 solution for the accreting gas in the total Jaffe potential of a given $T_{\rm V}$ can be built. In practice, the idea is to self-consistently "close" the model, determining a fiducial value for the gas temperature as a function of the galaxy model hosting accretion. In this approach, the steps to build an accretion solution are (1) choose M_*, r_*, μ, $\mathcal{R}_{\rm g}$, and $\xi_{\rm g}$ for a realistic galactic model; (2) obtain the gas virial temperature $T_{\rm V}$; and (3) derive $\mathcal{R}$ and ξ to be used in the Bondi problem and construct the corresponding CP17 solution.

Suppose the galaxy parameters in the first step are given. Then, for assigned $\mathcal{R}_{\rm g}$, $\xi_{\rm g}$, and μ, the parameter $\mathcal{R}$ in the accretion solution is obtained from Equations (12), (21), and (22) as

$$\mathcal{R} = \frac{\mathcal{R}_{\rm g}}{\mu} = \frac{\alpha \xi_{\rm g}}{\mu}, \tag{42}$$

where the last expression depends on the fact that we are restricted to the case $\xi_{\rm g} \geqslant 1$. Since $\mu \approx 10^{-3}$ and $\mathcal{R}_{\rm g}$ is expected (say) in the range $1 \div 20$, the $\mathcal{R}$ values fall in the range $10^3 \div 10^4$ (see also Section 5.1 for a more quantitative discussion).

From Equation (12), the second parameter (ξ) characterizing the accretion solution requires the computation of the Bondi radius $r_{\rm B}$ and then of the gas temperature T_∞; we choose $T_\infty = \beta T_{\rm V}$, with $\beta > 0$ a dimensionless parameter. Thus, the isothermal sound speed is given by

$$c_\infty^2 = \frac{kT_\infty}{\langle \mu \rangle m_{\rm p}} = \frac{\beta \sigma_{\rm V}^2}{3}, \tag{43}$$

and from Equations (3) and (41), the Bondi radius reads

$$\frac{r_{\rm B}}{r_*} = \frac{3\mu}{\alpha \beta \mathcal{F}_{\rm g}}, \quad \mathcal{F}_{\rm g} \equiv \xi_{\rm g} \widetilde{W}_{\rm g}(\xi_{\rm g}). \tag{44}$$

From the behavior of the function $\mathcal{F}_{\rm g}(\xi_{\rm g})$, it follows that at fixed α and β, one has

$$\frac{3\mu}{\alpha\beta} \leqslant \frac{r_{\rm B}}{r_*} \leqslant \frac{6\mu}{\alpha\beta}, \tag{45}$$

where the lower limit is obtained for $\xi_{\rm g} \to \infty$ and the upper limit for $\xi_{\rm g} = 1$; in this latter case, $\alpha = 1$ gives the value of $r_{\rm B}/r_*$ in a one-component (stellar) Jaffe galaxy. As expected, $r_{\rm B}$ decreases for increasing α, β, and $\xi_{\rm g}$, i.e., for increasing T_∞. Figure 2 (top left panel) shows the trend of $r_{\rm B}/r_*$ with $\xi_{\rm g}$ in the minimum halo case ($\alpha = 1$) and for $\alpha = 2$ and 3 when $\beta = 1$ and $\mu = 0.002$. Therefore, in a real galaxy with r_* of the order of a few kpc and a gas temperature of the order of $T_{\rm V}$, $r_{\rm B}$ is of the order of tens of pc (see also Section 5.1 for a more quantitative discussion). As additional information on $r_{\rm B}$, in Figure 2 (top right panel), we show the trend of $r_{\rm B}/R_{\rm inf}$ with $\xi_{\rm g}$ for $\beta = 1$; note that from Equations (37) and (44), the ratio is independent of α and μ, so that only one curve is plotted; higher values of β correspond to smaller values of $r_{\rm B}$.

Using Equations (12) and (44), we finally obtain the expression

$$\xi = \frac{\alpha\beta\xi_{\rm g}\mathcal{F}_{\rm g}}{3\mu} = \frac{\mathcal{R}\beta\mathcal{F}_{\rm g}}{3}. \tag{46}$$

It follows that $\xi \to \alpha\beta/(6\mu)$ for $\xi_{\rm g} \to 1$, while it grows without bound for $\xi_{\rm g} \to \infty$, as $\xi \sim \alpha\beta\xi_{\rm g}/(3\mu)$. In practice, at variance with the general cases in KCP16 and CP17, $\mathcal{R}$ and ξ are now linked, and increasing values of $\mathcal{R}$ correspond to increasing values of ξ. The list of all parameters introduced in this work is given in Table 2. Figure 2 (bottom left panel) shows the trend of ξ with $\xi_{\rm g}$ in the minimum halo case ($\alpha = 1$) and for $\alpha = 2$ and 3 and $\beta = 1$. Here $r_{\rm B}$ is of the order of $10^{-3} r_{\rm g}$; higher values of β correspond to larger values of ξ.

Having obtained the expressions for $\mathcal{R}$ and ξ as a function of the model parameters, a few considerations are in order. The first is that in JJ models, isothermal accretion is always possible in the absence of a central MBH and $\beta = 1$, because the accretion condition in Equation (17) is automatically satisfied by the virial temperature of the stellar component when $T_\infty = T_{\rm V}$. By allowing for a $T_\infty > T_{\rm V}$, it is easy to show that Bondi isothermal accretion in the absence of a central MBH (or when $\chi = 0$) is possible in JJ models only for gas temperatures lower than a critical value, i.e., only for $\beta \leqslant \beta_{\rm c} \equiv 3/(2\mathcal{F}_{\rm g})$.

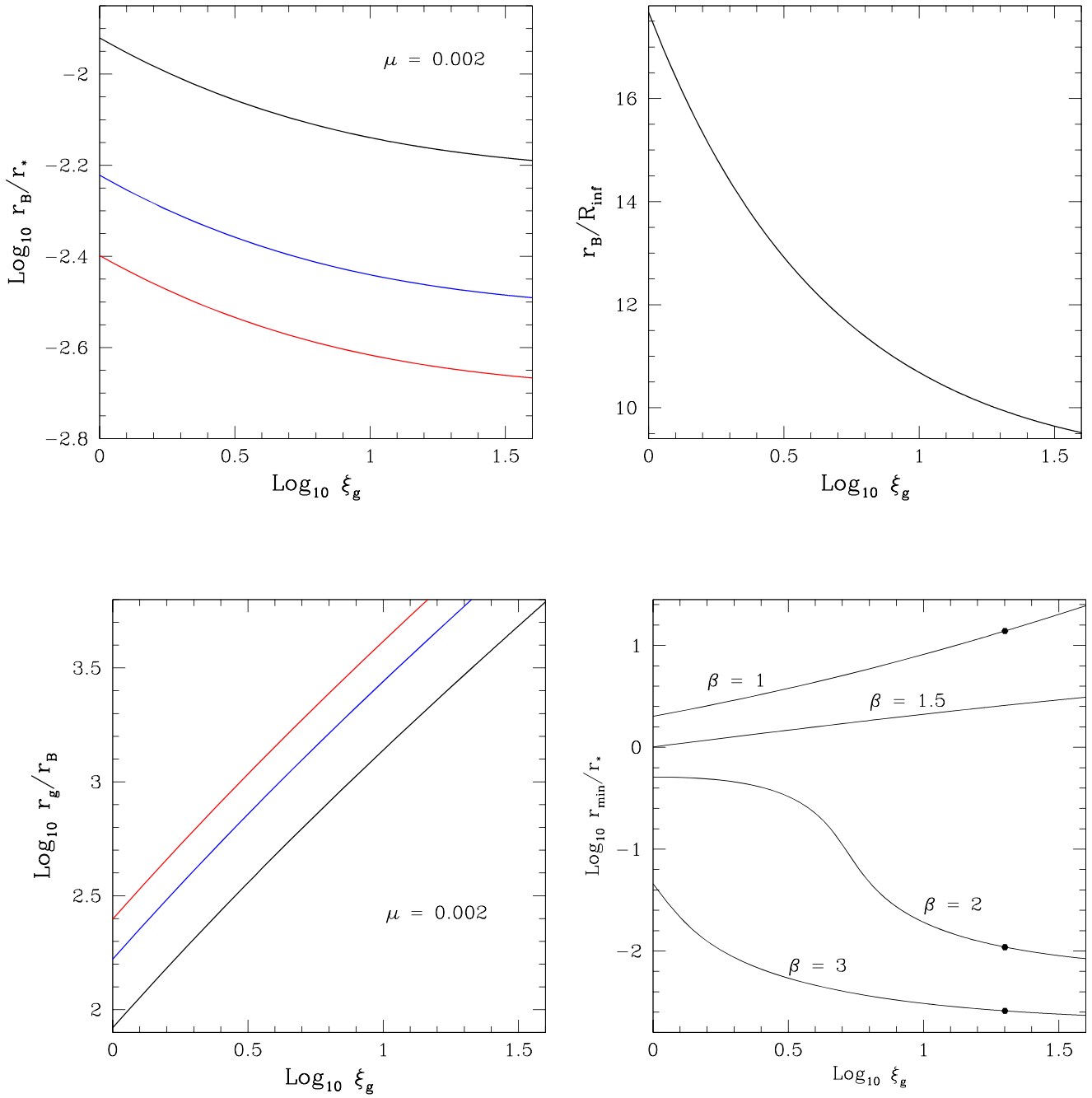

Figure 2. Relevant scale lengths of the isothermal accretion solution in JJ models as a function of $\xi_g = r_g/r_*$. An MBH-to-galaxy stellar mass ratio $\mu = 2 \times 10^{-3}$ is assumed, and $T_\infty = \beta T_V$. Top left: ratio r_B/r_* from Equation (44) with $\beta = 1$ and $\alpha = 1, 2, 3$, following the color scheme as in Figure 1. Top right: ratio r_B/R_{inf} of the Bondi radius to the radius of the sphere of influence of the MBH, R_{inf}, for $\epsilon = 0.5$ from Equations (37) and (44) with $\beta = 1$. Note that this ratio is independent of α and μ. Bottom left: parameter $\xi = r_g/r_B$ from Equation (46) with $\beta = 1$ and $\alpha = 1, 2, 3$. Bottom right: ratio r_{min}/r_* for $\alpha = 1$ and $\beta = 1, 3/2, 2, 3$. For large values of $\mathcal{R}$ and $\beta < \beta_c$, the ratio is almost independent of α but strongly dependent on gas temperature, as follows from Equations (44), (47), and (48). Filled circles ($r_{min}/r_* \simeq 13.84, 0.011, 0.0026$) mark the position of the sonic radius for the minimum halo case with $\xi_g = 20$.

From the behavior of $\mathcal{F}_g$, it follows that $3/2 \leqslant \beta_c \leqslant 3$, where the lower limit corresponds to $\xi_g \to \infty$ and the upper limit to $\xi_g = 1$. The second is that from Equation (46), the ratio $\mathcal{R}/\xi = 2\beta_c/\beta$ appearing in the definition of $f(x)$ in Equation (13) depends on β and ξ_g only, and it shows that for very large values of β, the problem reduces to the classical Bondi accretion.

The critical value β_c also plays an important role in models with a central MBH, determining a particular temperature at which there is a sudden transition in the position of the sonic radius. In fact, the location of r_{min} in terms of the scale length r_* is given by

$$\frac{r_{min}}{r_*} = x_{min}(\chi, \mathcal{R}, \xi)\,\frac{r_B}{r_*}, \tag{47}$$

where x_{min} is given by Equation (15) and can be easily computed analytically once $\mathcal{R}$ and ξ are determined. Figure 2 (bottom right panel) shows r_{min}/r_* as a function of ξ_g for $\alpha = 1$ and different values of β. The most relevant feature is the considerable variation in the position of r_{min}, from very external

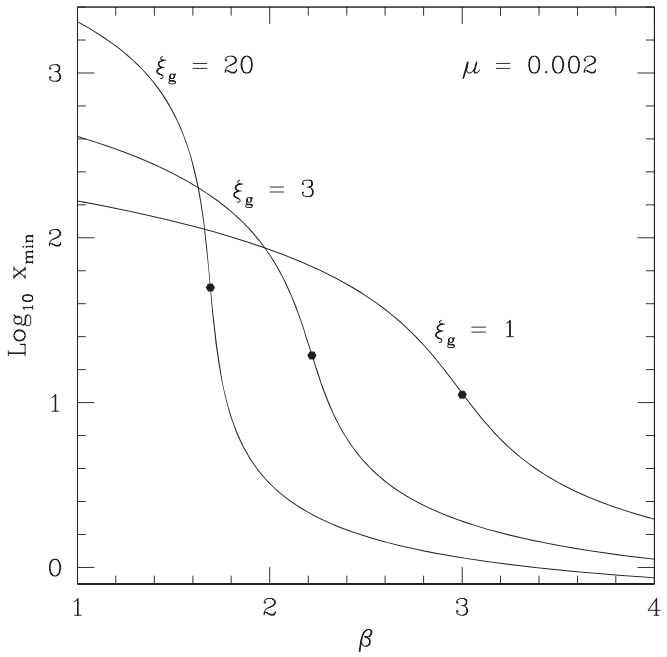

Figure 3. Position of x_{min} as a function of the temperature parameter β for $\mu = 0.002$ and three minimum halo models ($\alpha = 1$) with $\xi_g = 1$, 3, 20; these correspond to critical values of the temperature given by $\beta_c \simeq 3$, 2.2, 1.7, respectively (filled circles). The values of x_{min} are reproduced remarkably well by the asymptotic expressions in Equation (48).

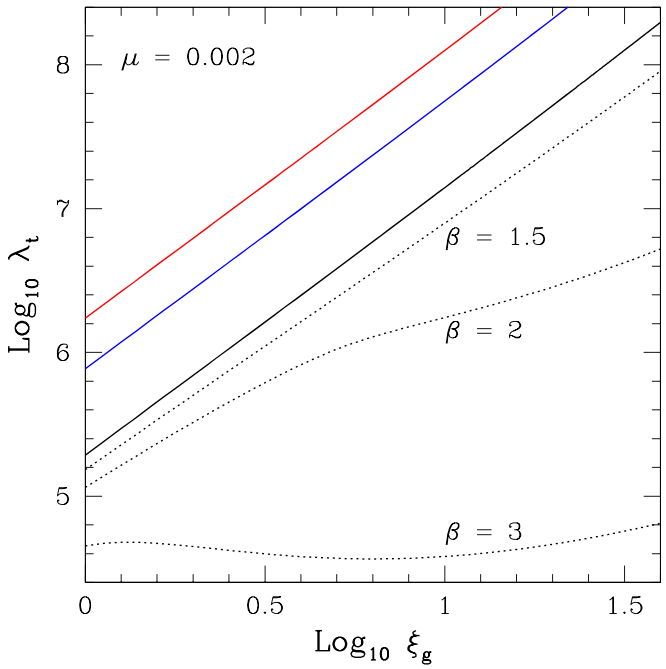

Figure 4. Critical accretion parameter λ_t as a function of ξ_g for the minimum halo case $\alpha = 1$ (black), 2 (blue), and 3 (red) and $\chi = 1$ and $\beta = 1$. The dotted curves refer to $\alpha = 1$ and three different values of β.

to very inner regions, for β increasing. Equation (47) shows that r_{min} is determined by the combined behavior of two functions, namely x_{min} and r_B/r_*; we now focus on x_{min}, having already established that $r_B \propto 1/\beta$, and thus the large variation of r_{min} can only be due in part to the dependence of r_B on β. Instead, from Equations (15), (42), and (46), for $\mathcal{R} \to \infty$ and fixed[3] β, x_{min} is given by

$$x_{min} \sim \begin{cases} \dfrac{\mathcal{R}\,(1-\beta/\beta_c)}{2}, & \beta < \beta_c, \\ \dfrac{\sqrt{\chi\mathcal{R}}}{2}, & \beta = \beta_c, \\ \dfrac{\chi}{2(1-\beta_c/\beta)}, & \beta > \beta_c. \end{cases} \tag{48}$$

Note that the limit $\mathcal{R} \to \infty$ describes models with increasing α at fixed μ and ξ_g, increasing ξ_g at fixed α and μ, or a vanishing MBH mass at fixed α and ξ_g. As in the present models, $\alpha \geqslant 1$, $\xi_g \geqslant 1$, and $\mu = 0.002$, then $\mathcal{R}$ is quite large, and the asymptotic trends in Equation (48) already provide a reasonable approximation of the true behavior that is increasingly better for large values of α and ξ_g and small values of μ. Of course, an independent check of the first two expressions above can be obtained by recovering them from the exact Equation (16) (pertinent to a Jaffe galaxy with $M_{BH} = 0$) by using Equations (42) and (46) for vanishing MBH mass, i.e., $\mu \to 0$, $\mathcal{R} \to \infty$, and $\beta \leqslant \beta_c$.

Qualitatively, Equation (48) shows that for $\beta < \beta_c$, x_{min} increases as $\mathcal{R}$. Instead, for $\beta > \beta_c$, x_{min} is independent of $\mathcal{R}$, and for very large values of the gas temperature tends to $\chi/2$, the limit value of classical Bondi accretion with electron scattering (e.g., CP17, see their Equation (25)). As Figure 3 shows, even a moderate increase in the gas temperature produces a sudden decrease in the value of x_{min}. A numerical investigation of polytropic accretion in JJ models shows that x_{min} suddenly drops to values $\lesssim 1$ as γ increases with respect to the isothermal case. This behavior is reminiscent of the sudden transition of x_{min} from external to internal regions in Hernquist galaxies, discussed in CP17; in this case, the transition is due to the existence, for $\gamma > 1$, of two minima for the polytropic function $f(x)$ of the Jaffe potential (as obtained by inserting Equation (11) into Equation (47) in KCP16). In the polytropic Hernquist case, the two minima can also be present in the isothermal case (CP17, Appendix B.2), while for the Jaffe potential in the isothermal case, there is only one minimum, given in Equation (15).

It is now easy to explain the behavior of the curves in Figure 2 (bottom right panel), where several cases of Equation (47) are plotted. For example, from the first identity in Equation (48) and Equations (42)–(44), Equation (47) predicts that for $\mathcal{R} \to \infty$ and $\beta < \beta_c$, we have $r_{min}/r_* \sim \xi_g(\beta_c/\beta - 1)$, so that for $\xi_g \to \infty$ and $\beta = 1$, it results in $r_{min}/r_* \sim \xi_g/2$, while for $\xi_g = 1$ and large values of α/μ, one has $r_{min} \approx 2r_*$. For T_∞ corresponding to the range $3/2 \leqslant \beta \leqslant 3$, there is a transition value of ξ_g such that, for larger ξ_g, β_c drops below the adopted β, and the third expression in Equation (48) applies. In these cases, the sonic radius moves to the central regions, with $r_{min}/r_* \sim \chi\mu/[\alpha(\beta/\beta_c - 1)]$.

Finally, Figure 4 shows the trend of λ_t as a function of ξ_g for $\alpha = 1$, 2, and 3 and, when $\alpha = 1$, for different gas temperatures as determined by the β value (dotted lines). In analogy with Equation (48), an asymptotic analysis shows that

[3] From Equation (46) $2\xi = \mathcal{R}\beta/\beta_c$, and from Equation (15), it follows immediately that the limit for $\mathcal{R} \to \infty$ is not uniform in β.

in the limit of $\mathcal{R} \to \infty$,

$$\lambda_t \sim \begin{cases} \frac{\mathcal{R}^2 (1-\beta/\beta_c)^{2-\frac{2\beta_c}{\beta}}}{4\sqrt{e}}, & \beta < \beta_c, \\ \frac{\mathcal{R}^2}{4\sqrt{e}}, & \beta = \beta_c, \end{cases} \tag{49}$$

and, for simplicity, we do not report the expression of λ_t for $\beta > \beta_c$, which can, however, be easily calculated. For fixed $\mathcal{R}$ and χ, very large β corresponds to $\lambda_t \sim \chi^2 \lambda_{cr}$, in accordance with the classical case (KCP16; CP17). Equation (49) nicely explains the values and trend of λ_t with ξ_g and α, in particular the almost perfect proportionality of λ_t to $\alpha^2 \xi_g^2$. From Equation (14), this implies that, for the same boundary conditions, the true accretion rate $\dot{M}_t$ for increasing ξ_g becomes much larger than $\dot{M}_B$, the rate in the sole presence of the MBH.

5. Two Applications

We present here two applications of the results above. The first is a practical illustration of how to determine the main parameters describing the galactic structure, and the gas accretion in it, for JJ models (see Table 2). One will see how very reasonable values for the main structural properties can be obtained, and then realistic galaxy models can be built. The second application considers the deviation from the true value of the mass accretion derived using the density along the accretion solution in JJ galaxies and the framework of classical Bondi theory.

5.1. Accretion in Realistic Galaxy Models

Here we show how to build JJ galaxy models with the main observed properties of real galaxies and how to derive the corresponding parameters for isothermal accretion.

The first step consists of the determination of the stellar component of the JJ galaxy. This is done via the choice of two main galaxy properties, for example, the effective radius R_e and the stellar projected velocity dispersion $\sigma_{gp}(0)$. For JJ models, $\sigma_{gp}(0) = \sigma_g(0)$, and $\sigma_g(r)$ is quite flat at the center; thus, $\sigma_{gp}(0)$ is very close to the emission-weighted projected stellar velocity dispersion within a small fraction of R_e (as typically given by observations). For a chosen R_e and $\sigma_{gp}(0)$, then, one has $r_* \simeq 1.34 R_e$ (see the comment below Equation (20)), and then M_* from Equations (21) and (32), once a value for $\alpha \geqslant 1$ is fixed. The central MBH enters the problem via a choice for μ that we take to be $\mu = 2 \times 10^{-3}$ (e.g., Kormendy & Ho 2013). Then the radius of influence R_{inf} can be evaluated from Equation (37). As an example, for a choice of $R_e = 5$ kpc and $\sigma_{gp}(0) = 210\,\mathrm{km\,s^{-1}}$, one has $r_* \simeq 6.7$ kpc, $\alpha M_* \simeq 1.38 \times 10^{11}\, M_\odot$, and $R_{inf} \simeq 4.6/\alpha$ pc, for a fiducial $\epsilon = 0.5$.

The second step consists of the determination of the parameters $\mathcal{R}_g$ and ξ_g that fix the total density distribution of the galaxy, in particular its total potential. Since $\mathcal{R}_g = \alpha \xi_g$, we can only fix either $\mathcal{R}_g$ or ξ_g. It may be convenient to fix ξ_g, for the following reason. A detailed dynamical modeling of stellar kinematical data for galaxies of the local universe has shown that the dark matter fraction within R_e is low (e.g., Cappellari 2016). To fit with this result, one can use Equation (28), which relates ξ_g and the dark matter fraction within any radius r; thus, for the desired (low) value of the dark matter fraction, ξ_g remains determined. Figure 1 shows that the ratio $M_{DM}(R_e)/M_g(R_e)$ is always in the range determined by the dynamical modeling for $\alpha = 1$. The figure also shows that, for $\xi_g \gtrsim 5$, the dark matter fraction within $r = R_e$ is quite independent of ξ_g. This means that a certain freedom remains in the choice of ξ_g, and we can further constrain it from other considerations. If $\alpha = 1$, we may require that the scale length of the dark halo (r_{NFW}) is larger than that of the stars (i.e., $\xi_{NFW} > 1$). For example, a value of the concentration parameter $c \simeq 10$, as predicted for galaxies of the local universe (e.g., Dutton & Macciò 2014), gives $\xi_{NFW} = 2.6$ for $\xi_g = 20$ (Equation (30)). Finally, one recovers the stellar virial velocity dispersion $\sigma_V^2 = 2\mathcal{F}_g(\xi_g)\sigma_{gp}^2(0)$ and then T_V from ${\sigma_V}^2$. Since $\mathcal{F}_g(\xi_g)$ varies only by a factor of two for $\xi_g = 1$ to ∞, in turn, T_V varies at most by a factor of two. For $\xi_g = 20$, one has $\sigma_V \simeq 280\,\mathrm{km\,s^{-1}}$ and $T_V \simeq 2.0 \times 10^6$ K (for $\langle\mu\rangle = 0.6$).

Having completely determined the galaxy structure with the choice of two observed quantities, R_e and $\sigma_{gp}(0)$, and three parameters (μ, α, ξ_g), the next step consists of the determination of the accretion properties. These are all fixed, once the galaxy structure is fixed; only the gas temperature needs to be chosen. The first parameter describing accretion is $\mathcal{R}$, obtained from Equation (42). The second parameter is ξ, which comes from Equation (46) once the parameter β is fixed in Equation (43). With the choice of this last parameter, i.e., with the choice of T_∞, all of the accretion properties are finally determined analytically, in particular the gas sound speed c_∞ (Equation (43)), Bondi radius r_B (Equations (3) and (44)), sonic radius r_{min} (Equations (15) and (47)), critical accretion parameter λ_t (as described after Equation (15)), and Mach number profile $\mathcal{M}$ (Equation (18)). As an example, for the galaxy model considered, for $\alpha = 1$, $\beta = 1$, and $\xi_g = 20$, one has $\mathcal{R} = 10^4$, $r_B \simeq 45$ pc, $\xi \simeq 2.96 \times 10^3$, $r_{min} \simeq 93$ kpc, and $\lambda_t \simeq 5.23 \times 10^7$. Instead, changing only the gas temperature to $\beta = 2$, one has $\mathcal{R}$ unchanged, $r_B \simeq 23$ pc, $\xi \simeq 5.91 \times 10^3$, $r_{min} \simeq 73$ pc, and $\lambda_t \simeq 2.85 \times 10^6$.

Figure 5 shows the Mach number profiles for accretion onto an MBH (the classic Bondi problem) and an MBH at the center of a JJ model for the minimum halo case and three values of β. For the three galaxy models, the top axis gives the radial scale in terms of r/r_*. Again, it is apparent how a modest increase in the gas temperature produces a dramatic decrease of r_{min}. Real galaxies show an average observed temperature T_X of their hot coronae (that here should be identified with T_∞) that implies for $\beta = T_\infty/T_V$ a value in the range ≈1–2.5 (Pellegrini 2011; Posacki et al. 2013). Moreover, β on average decreases for $\sigma_g(0)$ increasing, as $\beta \propto \sigma_g(0)^{-0.2}$ (see Figure 2 in Pellegrini 2011). In conclusion, the supersonic region of the flow is expected to increase for larger $\sigma_g(0)$ and to be confined within R_e or much less for $\beta \gtrsim 1$.

Figure 6 shows a comparison between the gas velocity profile and the stellar velocity dispersion profile for the JJ models in Figure 5. Notice that near the center, $\sigma_{BH} \sim r^{-1/2}$ and $\mathcal{M} \sim r^{-1/2}$, so that their ratio is a constant; it can be easily shown that this constant is $\sqrt{6\chi}$, independent of α, β, ξ_g, $\mathcal{R}_g$, and μ. In principle, then, the value of σ_{BH} close to the center of a galaxy is a proxy for the (isothermal) gas inflow velocity.

5.2. The Bias in Estimates of the Mass Accretion Rate

We investigate here the use of the classical Bondi solution in problems involving accretion onto MBHs residing at the center of galaxies. This use is common in the interpretation of

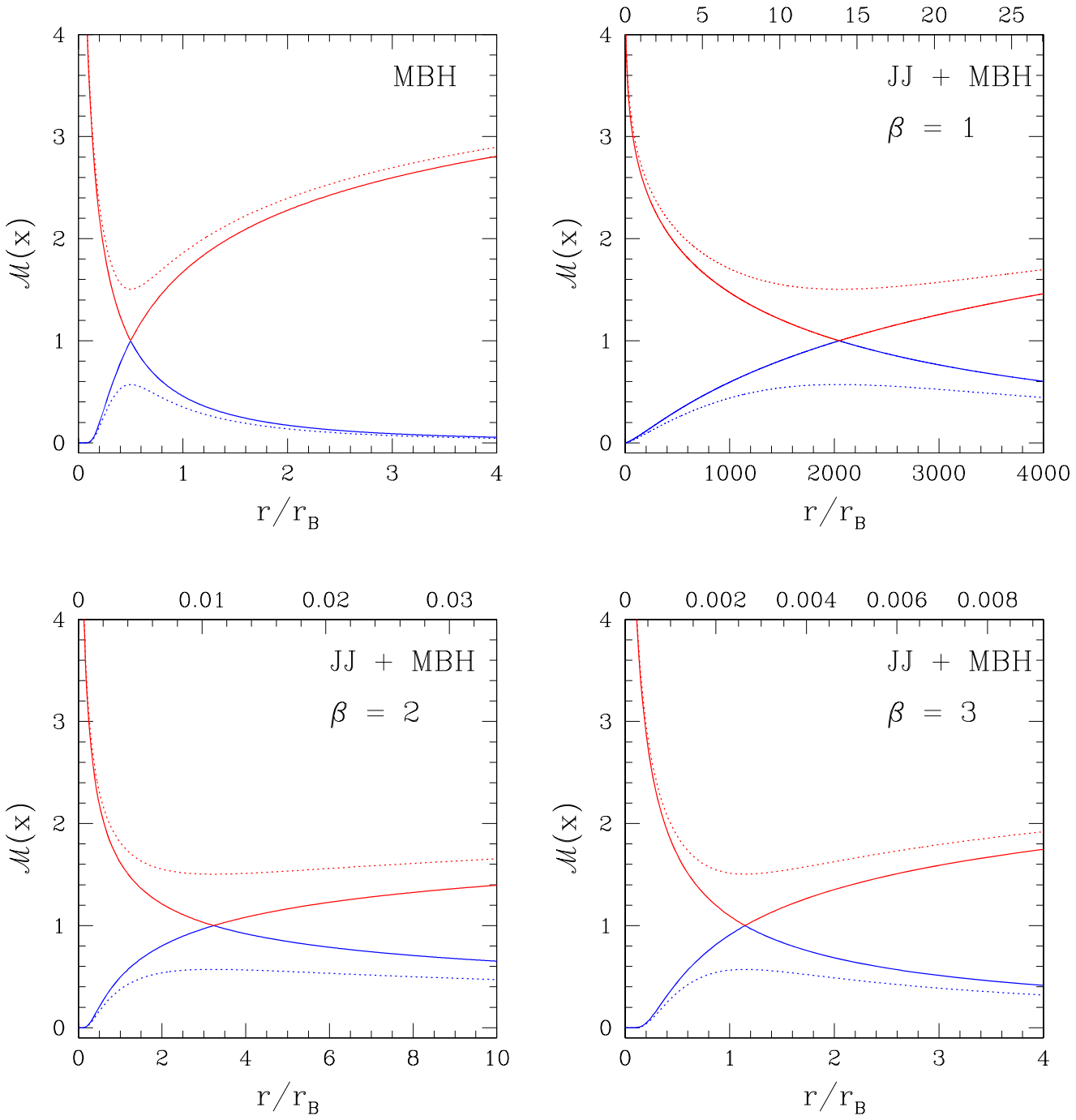

Figure 5. Mach number profiles as a function of $x = r/r_{\rm B}$ for isothermal Bondi accretion (with $\chi = 1$). The top left panel refers to classical Bondi accretion, and the other panels refer to accretion in a JJ galaxy model plus a central MBH with $\mu = 2 \times 10^{-3}$, $\mathcal{R}_{\rm g} = \xi_{\rm g} = 20$, and $\beta = 1$, 2, 3; the scale on the top axis gives the variable r/r_*. The subsonic regime is plotted in blue and the supersonic one in red. Solid lines show the two critical solutions, and dotted lines show the two subcritical solutions (with $\lambda = 0.8\lambda_{\rm cr}$ in the top left panel and $\lambda = 0.8\lambda_{\rm t}$ in the others).

observational results, numerical investigations, or cosmological simulations (see Section 1). In many such studies, when the instrumental resolution is limited or the numerical resolution is inadequate, an estimate of the mass accretion rate is derived using the classical Bondi solution, taking values of temperature and density measured at some finite distance from the MBH. This procedure clearly produces an estimate that can depart from the true value, even when assuming that accretion fulfills the hypotheses of the Bondi model (stationarity, spherical symmetry, etc.). KCP16 developed the analytical setup of the problem for generic polytropic accretion, with the inclusion of the effects of radiation pressure and a galactic potential; they also investigated numerically the size of the deviation for Hernquist galaxies. CP17 presented a detailed exploration of the deviation for isothermal accretion in one-component Jaffe and Hernquist galaxies. Here we consider the more realistic case of two-component JJ models in the isothermal case, exploiting the fully analytical character of JJ models.

We first consider the deviation of the estimate of the mass accretion rate for the classical Bondi solution when taking values of temperature and density measured at some finite distance from the MBH. For assigned values of ρ_∞, T_∞, γ, and

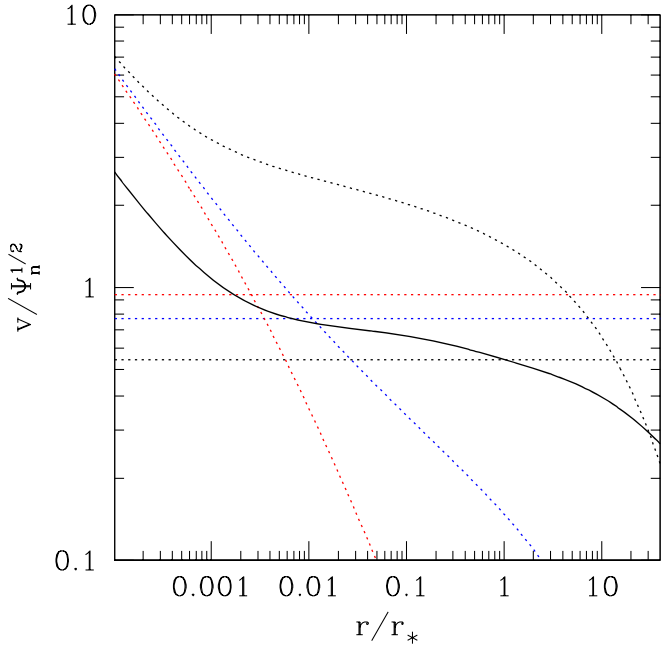

Figure 6. Accretion velocity profile for the gas (dotted) and isotropic stellar velocity dispersion profile (solid), both normalized to $\sqrt{\Psi_n}$, for the minimum halo model with $\mathcal{R}_g = \xi_g = 20$. The accretion solutions correspond to $\beta = 1$, 2, and 3 and are given by the black, blue, and red dotted lines, respectively. The horizontal dotted lines mark the corresponding values of $c_\infty/\sqrt{\Psi_n}$. For each β, the intersection between the accretion velocity and the sound velocity marks the sonic point (bottom right panel in Figure 2; filled circles).

M_{BH}, the Bondi radius r_B and the critical accretion rate $\dot{M}_B$ are given by Equation (3) and by Equation (5) with $\lambda = \lambda_{cr}$. If one inserts into these equations the values of $\rho(r)$ and $T(r)$ at a finite distance r from the MBH, taken along the classical Bondi solution, and considers them as "proxies" for ρ_∞ and T_∞, then estimated values for the accretion radius (r_e) and mass accretion rate ($\dot{M}_e$) are obtained:

$$r_e(r) \equiv \frac{GM_{BH}}{c_s^2(r)}, \quad \dot{M}_e(r) \equiv 4\pi r_e^2(r)\lambda_{cr}\rho(r)c_s(r). \tag{50}$$

The question is how much r_e and $\dot{M}_e$ depart from the true values r_B and $\dot{M}_B$ as a function of r. In the isothermal case, the sound speed is constant, with $c_s(r) = c_\infty$, and then $r_e(r) = r_B$, independently of the distance from the center at which the temperature is evaluated. Then $\dot{M}_e(r) = 4\pi r_B^2\lambda_{cr}\rho(r)c_\infty$; at infinity, $\dot{M}_e = \dot{M}_B$. At finite radii, instead

$$\frac{\dot{M}_e(r)}{\dot{M}_B} = \tilde{\rho}(x) = \frac{\lambda_{cr}}{x^2\mathcal{M}(x)}, \tag{51}$$

where the last identity comes from Equation (9), and $\mathcal{M}(x)$ is given in Equation (19) of CP17. The deviation of $\dot{M}_e$ from $\dot{M}_B$, then, is just given by $\tilde{\rho}(x)$ at the radius r where the "measure" is taken. Thus, $\dot{M}_e$ gives an overestimate of $\dot{M}_B$, and this overestimate becomes larger for decreasing x (see Figure 1 in KCP16 and Figure 4 in CP17).

In the presence of a galaxy, the departure of $\dot{M}_e(r)$ of Equation (50) from the true mass accretion rate $\dot{M}_t = 4\pi r_B^2\lambda_t\rho_\infty c_\infty$ is

$$\frac{\dot{M}_e(r)}{\dot{M}_t} = \frac{\lambda_{cr}\tilde{\rho}(x)}{\lambda_t} = \frac{\lambda_{cr}}{x^2\mathcal{M}(x)}, \tag{52}$$

where $\rho(r)$ is taken along the solution for accretion within the potential of the galaxy,[4] the last identity comes from Equation (19), and $\mathcal{M}(x)$ is given in Equation (18).

Figure 7 (left panel) shows the trend of $\dot{M}_e/\dot{M}_t$ with r. One sees that the use of $\rho(r)$ instead of ρ_∞ leads to an overestimate for r taken in the central regions, while $\dot{M}_e(r)$ becomes an underestimate for $r \gtrsim$ a few $\times 10^{-3} r_*$. The radius marking the transition from the region in which there is an overestimate to that in which there is an underestimate depends on the specific galaxy model. Figure 7 also shows the positions of r_B for the parameters chosen for the galaxy and accretion flow. Thus, in numerical simulations not resolving r_B, $\dot{M}_e$ should be boosted by a large factor to approximate the true accretion rate, $\dot{M}_t$. Moreover, since $\dot{M}_e/\dot{M}_t$ increases steeply with decreasing r, this "boost factor," in turn, also varies steeply with r. For example, for a representative distance from the center of 300 pc, for the same galaxy model considered in Section 5.1 with $r_* \simeq 6.7$ kpc, the boost factor suggested by Figure 7 varies between $\simeq$50 (for $\xi_g = 1$) and $\simeq$250 (for $\xi_g = 20$). For the same galaxy and a distance of 1 kpc from the center, the values are $\simeq$670 (for $\xi_g = 1$) and $\simeq$2000 (for $\xi_g = 20$). In the right panel of Figure 7, we also show the bias measured at the Bondi radius as a function of ξ_g. The panel indicates an underestimate by roughly a factor of 5.

It is instructive to find the reason for the trend of $\dot{M}_e$ near the center and at large radii. From Equation (52) and the expansion of $\mathcal{M}$ for $x \to 0^+$ and $x \to \infty$, one has

$$\frac{\dot{M}_e(r)}{\dot{M}_t} \sim \frac{\lambda_{cr}}{\sqrt{2\chi}\,x^{3/2}}, \quad x \to 0^+, \tag{53}$$

and

$$\frac{\dot{M}_e(r)}{\dot{M}_t} \sim \frac{\lambda_{cr}}{\lambda_t}, \quad x \to \infty. \tag{54}$$

Therefore, near the center, $\dot{M}_e/\dot{M}_t \sim r^{-3/2}$, while at large radii, as in general $\lambda_t \gg \lambda_{cr}$ (see Figure 4), $\dot{M}_e/\dot{M}_t$ becomes very small.

6. Summary and Conclusions

The classical Bondi accretion theory is the tool commonly adopted in many investigations where an estimate of the accretion radius and mass accretion rate is needed. In this paper, extending the results of previous works (KCP16; CP17), we focus on the case of isothermal accretion in two-component galaxies with a central MBH and radiation pressure contributed by electron scattering in the optically thin regime. In CP17, it was shown that the radial profile of the Mach number and the critical eigenvalue of the isothermal accretion problem can be expressed analytically in Jaffe and Hernquist potentials with a central MBH. Here we adopt the two-component JJ galaxy models presented in CZ18. These are made of a Jaffe stellar component plus a dark halo such that the total density is also described by a Jaffe profile; all the relevant dynamical properties of JJ models, including the solution of the Jeans equations for the stellar component, can be expressed analytically. Therefore, the results of CP17 and CZ18 give the opportunity of building a family of two-component galaxy

[4] In the monatomic adiabatic case $\gamma = 5/3$, one has that $\dot{M}_e(r) = \lambda_{cr}\dot{M}_t/\lambda_t$ independently of the distance from the center, while $r_e(r)$ departs from r_B (KCP16, see their Equation (42)).

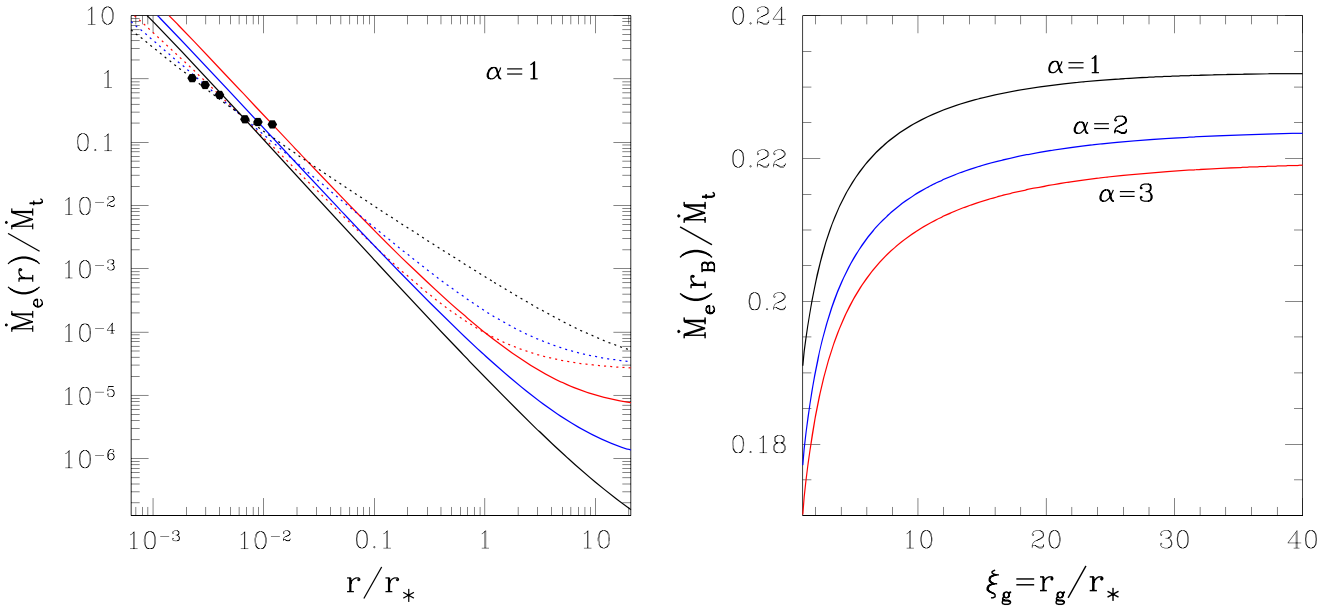

Figure 7. Left: ratio of the estimate of the accretion rate $\dot{M}_e$ and the true accretion rate $\dot{M}_t$, from Equation (52), as a function of r/r_* in the minimum halo case ($\alpha = 1$) for $\chi = 1$, $\beta = 1$, and $\xi_g = 1$ (red), $\xi_g = 3$ (blue), and $\xi_g = 20$ (black). The dotted lines correspond to $\beta = 3$, and the filled circles mark the position of the Bondi radius r_B in Equation (44). Right: ratio $\dot{M}_e/\dot{M}_t$ evaluated at r_B as a function of ξ_g for three values of α and $\chi = 1$, $\beta = 1$. In both panels, $\mu = 0.002$.

models where all the accretion properties can be given analytically and then explored in detail, with no need to resort to numerical studies. The main results of this work can be summarized as follows.

(1) The parameters describing accretion in the hydrodynamical solution of CP17 ($\mathcal{R}$ and ξ) have been linked to the galaxy structure. In particular, it is assumed that the isothermal gas has a temperature T_∞ proportional to the virial temperature of the stellar component, T_V. Then, simple formulae are derived relating the galactic properties (as the effective radius, R_e, and the radius of influence of the MBH, R_{inf}) with those describing accretion (as the Bondi radius, r_B, and the sonic radius, r_{min}). The critical accretion parameter λ_t is also expressed as a function of the galactic properties.

(2) For realistic galaxy structures, r_B is of the order of a few $\times 10^{-3} r_*$, and R_{inf} is of the order of $\simeq 0.1 r_B$. For $T_\infty = T_V$, the sonic radius r_{min} is of the order of a few R_e. For moderately higher values of T_∞, r_{min} suddenly drops to radii within r_B. The same also happens for a small increase of the polytropic index above unity, and this behavior is reminiscent of the similar jump shown by r_{min} in Hernquist models, as discussed in CP17. As a consequence, accretion in JJ models can switch from being supersonic over almost the whole galaxy to being subsonic everywhere, except for $r \lesssim r_B$. An explanation for this phenomenon is given.

(3) As for the isothermal accretion in one-component Jaffe models, the determination of the critical accretion parameter involves the solution of a quadratic equation, and there is only one sonic point for any choice of the parameters describing the galaxy. In the presence of the galaxy, λ_t is several orders of magnitude larger than without the galaxy. It is found that Bondi accretion in JJ models in absence of a central MBH (or when $\chi = 0$) is possible, provided that T_∞ is lower than a critical value and we derive the explicit formula for it. This critical value depends only on ξ_g and is in the range $3/2 \leqslant T_\infty/T_V \leqslant 3$. It also determines the jump in r_{min} in models with the central MBH.

(4) We provide a few examples of accretion in realistic galaxy models and present the resulting Mach number profiles and the trends of the accretion velocity and isotropic stellar velocity dispersion profiles.

(5) We finally examine the problem of the deviation from the true value $\dot{M}_t$ of an estimate of the mass accretion rate $\dot{M}_e(r)$ obtained adopting the classical Bondi solution for accretion onto an MBH, where the gas density and temperature at some finite distance from the center are inserted as proxies for their values at infinity. The size of the departure of $\dot{M}_e(r)$ from $\dot{M}_t$, which is determined by the presence of the galaxy, is given as a function of the distance r from the center. Here $\dot{M}_e(r)$ overestimates $\dot{M}_t$ if the gas density is taken in the very central regions and underestimates $\dot{M}_t$ if it is taken outside a few Bondi radii. This shows the sensitivity to the model parameters of the determination of a physically based value for the so-called "boost factor" adopted in simulations, and that in general, a universally valid prescription is impossible.

We thank the referee for useful comments that improved the presentation.

ORCID iDs

Luca Ciotti https://orcid.org/0000-0002-5708-5274
Silvia Pellegrini https://orcid.org/0000-0002-8974-2996

References

Barai, P., & de Gouveia Dal Pino, E. M. 2018, MNRAS, in press (arXiv:1807.04768)
Barai, P., Proga, D., & Nagamine, K. 2011, MNRAS, 418, 591
Barai, P., Proga, D., & Nagamine, K. 2012, MNRAS, 424, 728
Beckmann, R. S., Slyz, A., & Devriendt, J. 2018, MNRAS, 478, 995
Bondi, H. 1952, MNRAS, 112, 195
Bu, D.-F., Yuan, F., Wu, M., & Cuadra, J. 2013, MNRAS, 434, 1692
Cao, X. 2016, ApJ, 833, 30
Cappellari, M. 2016, ARA&A, 54, 597
Cappellari, M., Romanowsky, A. J., Brodie, J. P., et al. 2015, ApJL, 804, L21
Carollo, M., van der Marel, R., & de Zeeuw, P. T. 1995, MNRAS, 276, 1131

Choi, E., Ostriker, J. P. O., Naab, T., et al. 2017, MNRAS, 844, 31
Ciotti, L. 1999, ApJ, 520, 574
Ciotti, L., Lanzoni, B., & Renzini, A. 1996, MNRAS, 282, 1
Ciotti, L., Morganti, L., & de Zeeuw, P. T. 2009, MNRAS, 393, 491
Ciotti, L., & Ostriker, J. P. 2012, in Hot Interstellar Matter in Elliptical Galaxies, Vol. 378 ed. D.-W. Kim & S. Pellegrini (New York: Springer), 83
Ciotti, L., & Pellegrini, S. 2017, ApJ, 848, 29, (CP17)
Ciotti, L., & Ziaee Lorzad, A. 2018, MNRAS, 473, 5476, (CZ18)
Dehnen, W. 1993, MNRAS, 265, 250
Di Matteo, T., Colberg, J., Springel, V., Hernquist, L., & Sijacki, D. 2008, ApJ, 676, 33
Dutton, A. A., & Macciò, A. V. 2014, MNRAS, 441, 3359
Frank, J., King, A., & Raine, D. 1992, Accretion Power in Astrophysics., Vol. 21 (Cambridge: Cambridge Univ. Press)
Gallo, E., Treu, T., Marshall, P. J., et al. 2010, ApJ, 714, 25
Hernquist, L. 1990, ApJ, 356, 359
Jaffe, W. 1983, MNRAS, 202, 995
Kormendy, J., & Ho, L. C. 2013, ARA&A, 51, 511
Korol, V., Ciotti, L., & Pellegrini, S. 2016, MNRAS, 460, 1188, (KCP16)
Lusso, E., & Ciotti, L. 2011, A&A, 525, 115
Merritt, D. 1985, AJ, 90, 1027
Mościbrodzka, M., & Proga, D. 2013, ApJ, 767, 156
Navarro, J. F., Frenk, C. S., & White, S. D. M. 1997, ApJ, 490, 493
Park, K.-H., Wise, J. H., & Bogdanović, T. 2017, ApJ, 847, 70
Pellegrini, S. 2010, ApJ, 717, 640
Pellegrini, S. 2011, ApJ, 738, 57
Posacki, S., Pellegrini, S., & Ciotti, L. 2013, MNRAS, 433, 2259
Rafferty, D. A., McNamara, B. R., Nulsen, P. E. J., & Wise, M. W. 2006, ApJ, 652, 216
Ramírez-Velasquez, J. M., Sigalotti, L., Di, G., et al. 2018, MNRAS, 477, 4308
Sijacki, D., Springel, V., Di Matteo, T., & Hernquist, L. 2007, MNRAS, 380, 877
Tremaine, S., Richstone, D. O., Byun, Y.-I., et al. 1994, AJ, 107, 634
Volonteri, M., Capelo, P. R., Netzer, N., et al. 2015, MNRAS, 449, 1470